Fibers and Polymers 2016, Vol.17, No.8, 1277-1286
DOI 10.1007/s12221-016-6279-0

ISSN 1229-9197 (print version)
ISSN 1875-0052 (electronic version)

Preparation, Functional Characterization and Hemostatic Mechanism Discussion for Oxidized Microcrystalline Cellulose and Its Composites

Weilu Cheng[1,2], Jinmei He[1], Menglin Chen[2], Dalong Li[1,2], Hui Li[3], Lei Chen[1], Ye Cao[3], Jing Wang[3], and Yudong Huang[1]*

[1]*State Key Laboratory of Urban Water Resource and Environment, School of Chemistry and Chemical Engineering, Harbin Institute of Technology, Harbin 150001, China*
[2]*Interdisciplinary Nanoscience Center (iNANO), Aarhus University, Aarhus DK-8000, Denmark*
[3]*Department of Oral and Maxillofacial Surgery, The Second Affiliated Hospital of Harbin Medical University, Harbin 150001, China*

(Received February 29, 2016; Revised June 16, 2016; Accepted June 19, 2016)

Abstract: Effective and affordable hemostatic materials are of great interests in the development of biomaterials. Lignocellulose, which is a raw material for microcrystalline cellulose, is one of the most economical and readily available polymers in the nature. The oxidized microcrystalline cellulose particles prepared in NO_2/CCl_4 oxidation system may be a type of affordable, effective and nontoxic hemostatic biomaterial. The FT-IR and ^{13}C solid state NMR results showed that the hydroxyl groups on C6 of cellulose were highly selectively oxidized. The increase of carboxyl content and Zeta potential of OMCC were highly dependent on the oxidation time at the first 64 h. XRD spectra indicated that the crystallinity changed from 70.01 % (MCC) to 60.63 % (OMCC-96 h), and the particle size decreased to 80 μm (OMCC-96 h). To composite with oxidized regenerated cellulose gauze, the OMCC-64 h was optimal, based on the dramatically reduced DP value after 64 h oxidization. The results showed this novel composite with negative charge exhibited good hemostatic property and antibacterial activity. The composite was possessed of both the good biocompatibility for mouse endothelial cells in vitro and the superior biodegradation for rabbits in vivo. Moreover, the data of enzyme-linked immunosorbent assay and blood coagulation tests in vitro suggested that the composite could adsorb and activate the platelets, and then the platelet glycoprotein (GPIIb/IIIa) receptor became competent to bind soluble fibrinogen. The composite also greatly accelerated the activation of the blood coagulation factor XII, and promoted the generation of thrombin, so that the extrinsic route of blood coagulation was initiated.

Keywords: Oxidation, Microcrystalline cellulose, Hemostasis, Antibacterial activity

Introduction

Cellulose as one of the crystalline structural polysaccharides accumulates as the most abundant biopolymer presented primarily in wood biomass [1,2]. There are more than 100 cellulose derivatives, and the viscose fiber is one of the most widely used in the world. Oxidized cellulose is the most valuable derivative product from viscose, and there are different types of oxidized cellulose that can be obtained under different oxidizing conditions [3,4]. Oxidized cellulose (OC) and Oxidized regenerated cellulose (ORC) with carboxyl groups on the C6 can be used as hemostatic material in the medical field due to its good biocompatibility and degradability [5,6]. At present, the most widely used clinical application is the Johnson & Johnson's products - medical absorbable hemostatic gauze called *Surgicel*® [7,8]. Our laboratory has also prepared ORC and oxidized regenerated cellulose sodium (ORC-Na) with excellent hemostatic effect [9,10]. With a large microscopic size, ORC is not good at the rapid absorption of blood, which needs 2-8 minutes to stop bleeding after contacting with wounds [10]. Therefore, ORC is much more suitable for the small wounds and not effective enough for serious bleeding site [11]. On the other hand, viscose fiber which is the raw material to synthesize ORC, is easy to expand when it meets the liquid. And there is a serious waste of oxidation liquid and a high costing of production, due to the fact that the viscose fiber is a combination of amorphous and crystallographic cellulose [2,12].

Microcrystalline Cellulose (MCC) is another type of widespread used cellulose derivatives, whose concept is proposed by Battista *et al.* in 1950s to 1960s [1,13]. MCCs are small, white or off white, odorless and tasteless, dried, porous particles, which are insoluble in water, dilute acid, dilute sodium hydroxide and most organic solvents [14,15]. The size of MCC is around 20-80 μm, and its limiting degree of polymerization is 15-375. Compared with viscose, MCC is characterized by higher degree of crystallinity and deformation, lower degree of polymerization, and less fibrous as its crystallographic structure [16,17]. Because of its morphological structure, MCC has some very unique physicochemical properties including water imbibition, liquidity and compressibility, etc [18,19]. Due to these properties, MCC has been extensively used in medicine and health care, food, light industry, daily chemical and other fields, and it should become a cheap natural polymer functional material applied in more and more fields [14,19].

Microcrystalline cellulose has a lower swelling rate, a

*Corresponding author: ydhuang.hit1@aliyun.com

smaller material size and a higher specific surface area, which have contribution to prepare the cheap and effective hemostatic material with saving oxidation liquid and a simple and effective method [13,20]. For these reasons, we attempted to use the cheap food-grade microcrystalline cellulose to synthesize a new product of OC with microstructure and prepare the composite with good hemostatic properties by multi-step processing. Meanwhile, we conduct characterization of the hemostatic particles and composite. At the same time, the hemostatic mechanism of this composite was investigated preliminarily by Zeta potential, platelets meter, auto-hemagglutinin meter and enzyme-linked immunosorbent assay. In addition, a series of specialized experiments were applied to assess its biological compatibility and biological availability.

Experimental

Materials

Microcrystalline cellulose (DP=135) was obtained from Shanghai Chineway Pharmaceutical Technology Co., Ltd., Shanghai, China. NO_2 (AR) was purchased from Summit Specialty Gases Co., Ltd., Tianjin city, China. CCl_4 (AR) was received from Shuang Shuang Chemical Co., Ltd., Yantai, China. Ethanol (AR) was purchased from Fu Yu Chemical Co., Ltd., Tianjin, China. Ultra-pure water was purchased from Xinyue Chemical Co., Ltd., Weihai, China. The male New Zealand white rabbits, human and rabbit fresh blood anticoagulated with sodium citrate were all supplied by the Second Affiliated Hospital of Harbin Medical University (Harbin, Heilongjiang Province, China). All of the kits for enzyme-linked immunosorbent assay were purchased from R&D Systems Inc. Mouse endothelial cells, bovine serum and penicillin were provided by Sanggon biotech Co. (Shanghai, PR China). The protocol was approved by the Ethics Committee of the Sencond Affiliated Hospital of Harbin Medical University. All animals were handled in accordance with the Chinese National Institutes of Health Guidelines for the Care and Use of Laboratory Animals.

Preparation of the Oxidized Microcrystalline Cellulose (OMCC)

To activate the MCC, which was a type of food-grade raw material, it should be washed three times with the ultra-pure water and dried under 50 °C for 6 h. The oxidation process of MCC was performed by using the solution of 35 % nitrogen dioxide in CCl_4. The ratio of MCC to solution volume was 1:36.2 (g/m*l*) with excess NO_2. The MCC was immersed at 19.5 °C in the solution with stirring for different time varying from 24, 48, 64 and 80 to 96 h (oxidized samples denoted as OMCC-24 h, OMCC-48 h, OMCC-64 h, OMCC-80 h, OMCC-96 h). The OMCC was cleaned three times by vacuum filtration with 100 % CCl_4, 45-55 (volume) % of ethyl alcohol aqueous solution and 100 % ethyl alcohol sequentially and respectively. Then the OMCC was placed in a freeze-dryer in order to remove all the water from it over the course of 24 h, and should be stored at 0-4 °C.

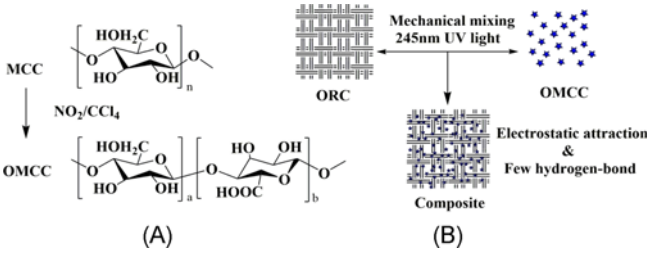

Figure 1. The chemical reaction equation of OMCC and the sketches of hemostatic composite preparation.

Preparation of Hemostatic Composite

The OMCC was equably dispersed in ethanol by ultrasonic method, and the ratio of the OMCC to ethanol volume was 1:2.5 (g/m*l*). Immersed the ORC gauze in the OMCC/ethanol solution for 2 hours, then picked up the ORC/OMCC-64 h gauze and gave 245 nm ultraviolet light for 30 minutes. After washed for 3 times by ethanol, the ORC/OMCC-64 h hemostatic composite was prepared, and the ratio of OMCC to ORC was 1:20 (g/g). Due to the hydrogen bond and static electricity action between the OMCC and ORC [21-23], the hemostatic composite had a well combinability (shown in Figure 1).

Characterization

Fourier Transform Infrared Spectroscopy (FTIR) was obtained with a Nicolet-Nexus670 spectrophotometer in the reflection mode. Solid state ^{13}C NMR spectra were recorded on Bruker Avance 400 WB spectrometer equipped with a 4 mm standard bore CP/MAS probe head (magnetic field ¼ 9.4 T, 13C frequency ¼ 100.12 MHz) at room temperature. The spinning rate and the contact time were 10.0 kHz and 3.0 ms, respectively. Each dried and powdered sample was scanned for 1000 times, and recorded with 6 s recycle delay. XRD measurement was carried out by a D/man-rBX X-ray generator operated at 30 mA and 40 kV. The Zeta potential was measured by a Malvern Zetasizer. The particle size was got from a Laser Particle Size Analyzer (Saturn DigiSizer 5200). The Scanning electron microscopy (SEM) observation was obtained from a Hitachi S-4700 SEM. The specific surface area was determined by the Brunauer-Emmett-Teller (BET) method using the data between 0.01 and 0.99. The pore size distributions was derived from the desorption branches of the isotherms using the Barrett-Joyner-Halanda (BJH) method.

Determination of Carboxyl Content and Degree of Polymerization (DP)

Carboxyl content was measured according to United

States Pharmacopoeia. Firstly, 2 % calcium acetate and 0.1 M NaOH solutions were prepared. Then, 0.5 g ORC (cut into short fibers) or OMCC was soaked with 50 m*l* solution of 2 % calcium acetate for 15 h. Using phenolphthalein as the indicator, the mixture was titrated with 0.1 M NaOH solution. And the consumed volume of NaOH was corrected for the blank. Such carboxyl content was calculated from the following equation:

$$\text{-}COOH\ (\%) = \frac{N \times V \times MW_{COOH}}{m} \times 100 \quad (1)$$

where N is the normality of 0.1 M NaOH solution, V is the consumed volume of NaOH which is corrected for the blank, MW_{COOH} is the molecular weight of carboxyl group and m is the weight of the sample.

DP of the ORC or OMCC was determined by ASTM. The detailed process was described as following: 0.4 g sample was accurately weighted and suspended in 25 m*l* water in a 125 m*l* erlenmeyer flask. Subsequently, 25 m*l* of 1.0 M cupriethylenediamine hydroxide (cuen) solution was added. The flask was sealed and shaken at room temperature for 30 min until the sample was completely dissolved. Thus, 0.8 g/100 m*l* ORC or OMCC solution was obtained. 10 m*l* of this solution was filled into an Osteald-Fenske capillary viscometer (size 100), and equilibrated the solution at 25 °C for about 15 min. Then, the efflux time was measured when the solution flowed between the two marks on the viscometer, and the the similar procedure was performed on 0.5 M cuen solvent. The relative viscosity could be obtained from the following equation:

$$\eta_r = \frac{Efflux-time_{solution}}{Efflux-time_{solvent}} \quad (2)$$

According to η_r, $[\eta]C$ values of cellulose samples could be obtained from the literature. Finally, the intrinsic viscosity $[\eta]$ corresponding to $[\eta]C$ could be utilized to calculate the DP as the following relationship:

$$DP = 190[\eta] \quad (3)$$

All values of carboxyl content and DP were measured for six times, and the results were showed as mean value±SD (N=6, X±S, *P<0.05).

Cell Viability

The cell viability was determined using a cell counting kit (CCK-8, Dojindo, Japan). Single cell suspensions containing 5000 mouse endothelial cells in 100 μl Dulbecco's Modified Eagle's Medium (DMEM, Invitrogen, with 4.5 g/*l* D-Glucose L and 4.5 M L-Glutamine) which was supplemented with 10 % FBS and 1 % penicillin-streptomycin (Invitrogen), was added in the 96-well plate and incubated for 48 h at 37 °C under 5 % CO_2. Then, 10 μl of different material extracting solutions (material/PBS, 1 g/1 m*l*, w/v) and 90 μl DMEM were added and incubated for 12 h, 24 h and 48 h.

The CCK-8 reagent was diluted to a 1/20 ratio with the cell culture medium. 300 μl of the mixture was pipetted into each well. After 2 h cultured, 100 μl of the mixture was transferred into a 96-well plate, and the absorbance was determined at 450 nm. Each experiment was performed in six replicate wells and independently repeated for three times.

Hemostatic Evaluation and Biodegradation in vivo

Male New Zealand White rabbits (which are 4 months old and around 3.5 kg) were used to evaluate the amount of excess blood which oozed out during the hemostat formation and the biodegradation period. Since these factors were difficult to be controlled in animal experiments, we used 10 rabbits for each sample to minimize the effect of the experimental error and choosed different experiment models. The hemostatic materials were cut into pieces of required size (1.0 cm×1.0 cm×0.1 cm) and sterilized by the 254 nm ultraviolet light for 30 min. All procedures were performed under sterile conditions.

Prior to an abdominal incision, the rabbits were fixed on the surgical cork board and anaesthetized with an intraperitoneal injection of 3 % pentobarbital sodium aqueous solution (30 mg/kg). Serous fluid was carefully removed because it would affect the estimation of the weight gained by the filter paper. Placed the parafilm and the filter paper which were pre-weighted by a balance beneath the liver (parafilm prevents the samples paper's absorption of gradually oozing blood). The cork board was tilted and maintained at an angle of about 45 to assist the flow of the bleeding from the liver towards the filter paper. In this step, the hemostatic composites were respectively applied to the liver wound immediately after the liver was pricked with a needle (the diameter is 2 mm, and the pricked depth is 3 mm). The hemostatic time and amount of bleeding were recorded till the bleeding was stopped. All values of hemostatic time and amount of bleeding were measured for six times, and the results were showed as median value±SD (N=6, X±S, *P<0.05).

After the anesthesia, the operational area was sterilized, and then a piece of testing hemostatic materials was implanted flat across the implantation site in one rabbits' leg muscle for 2 and 4 weeks, and each sample was repeated for six times to reduce the experiment errors. Then, the gentamicin (20,000 U/kg) was injected intramuscularly every two days for the first week. All the animals were intensively cared until the implanting terminals were reached. At each termination of the experimental period, the animals were sacrificed with overdose pentobarbital sodium. The implants and the surrounding tissues were taken out and fixed by 20 % formalin for macroscopic observation and histopathological evaluation. After gradient ethanol dehydrated, the specimens were embedded in paraffin, and cut into 2 μm-thick sections, then the nuclei and cytoplasm were stained with hematoxylin

and eosin (H&E). Then, the stained sections of each test sample were examined by light microscopy and photographed with a digital camera. The histopathologic photographs were reviewed by pathologist, who was working in The Second Affiliated Hospital of Harbin Medical University.

Antibacterial Activity Text

We used the gram positive bacterium, *Staphylococcus aureus* (*S. aureus*) - ATCC 6538 and gram negative bacterium, *Escherichia coli* (*E. coli*) - ATCC 8739 as test organisms. A tryptone soya agar (from Oxoids) was used as the nutrient agar for agar plates. The bacterial inoculums were prepared to get a bacterial suspension in exponential growth of 10^8 colony forming units (CFU) ml^{-1} in 5 m*l* of nutrient broth (modified Trypton soya broth from Oxoids).

Antibacterial test (performed according to the AATCC 100-2004 test standard) was carried out on control group (without any materilas), normal gauze, ORC, OMCC and the hemostatic composite. The circular fabric swatches were cut into 4 cm in diameter, sterilized under Co^{60} irradiation, and placed in a conical flask.

A series of diluted solutions were prepared as 10^0, 10^1, 10^2 and 10^3 times with sterile distilled water and they were plated (3 of each) and incubated for 18 hours at 37 °C. And then, we compared the treated and untreated swatches with the 10^2 dilution. The plates corresponding to 10^0 and 10^1 times had uncountable colonies and that for 10^3 times had too few colonies for the untreated control swatch. The percent reduction of the bacteria by the gauze specimen treatment was calculated with the following formula:

$$\text{Reduction in CFU (\%)} = (C - A)/C \times 100\ \%$$

where, C is average number of bacterial colony in normal gauze, A is average number of bacterial colony in other different samples

Blood Detections in vitro

In vitro platelets adhesion assay, rabbit platelets concentrate was the top layer of lemon-yellow plasma separated from the whole blood which was centrifuged 8 min at 1000 r.p.m at 22 °C. The OMCC was immersed in the phosphate buffer solution (PBS, pH=7.4) for 48 h to get the samples with different concentration (0.5 %, 1 %, 2 %). Then 0.2 m*l* samples or PBS were put into 1.8 m*l* platelets concentrate at 37 °C to immerse for 10 min, and measured the platelets adhesion rate with a Platelet Adhesion Meter, manufactured by Beijing Dongfangpulisheng Technology & Trade Co. Ltd.

In order to get the data of activited partial thromboplastin time (APTT), pro-time prothrombin time (PT) and thrombin time (TT), we put 0.2 m*l* samples or PBS into 1.8 m*l* whole rabbit blood at 37 °C and quickly detected them with C2000 auto-hemagglutinin meter, manufactured by Beijing Dongfangpulisheng Technology & Trade Co. Ltd.

The ELISA (Enzyme-linked immunosorbent assay) was allowed for the determination of different factors concentrations in human blood, such as beta thromboglobulin (β-TG), platelet factors 4 (PF4), platelet glycoprotein (GPIIb/IIIa) and activation of clotting enzymes factor XII (hagmeman factor, FXIIa). Purified human factors antibody was coated microtiter plate wells to obtain solid-phase antibody, then added samples (sample powders: blood=1 mg: 5 m*l*) to wells. The factor combined with antibody was labeled with horseradish peroxidase (HRP), and then it became antibody-antigen-enzyme-antibody complex. After washing completely, we added tetramethylbenzidine (TMB), and it became blue color anti-HRP enzyme-catalyzed. The reaction was terminated by the addition of a sulphuric acid solution and the color changes were measured spectro-photometrically at a wavelength of 450 nm using a Biotek (Winooski, VT) microplate spectro-photometer. The concentrations of factors in the samples were determined by comparing the O.D. of the samples to the standard curves.

Statistical Analysis

All data were represented as mean±standard deviation (SD). Statistical comparisons were performed using one-way ANOVA with post hoc tests. Differences were considered significant for $P<0.05$.

Results and Discussion

Chemical and Physical Structure Analysis

The FT-IR analyses of MCC and OMCC with different oxidation time were presented in Figure 2(A). The absorption peak refering to hydroxyl groups of ORC was assigned at 3200-3400 cm^{-1}, and the peak at 2900 cm^{-1} and 1650 cm^{-1} were due to the stretching vibration of -CH_2 and the bending vibration of O-H, respectively. The peak around 1739 cm^{-1} was due to the stretching vibration of C=O, which showed that the MCC was oxidized [12,24]. ^{13}C solid state NMR spectroscopy analysis was applied to identify which carbon atom was oxidized. From Figure 2(B), it was indicated that there was no change for the peaks of C1 at 104 ppm, C2, C3 and C5 were all around 72-78 ppm, and the shoulder signal from 84 to 89 ppm were due to crystalline and amorphous C4. Comparing with NMR spectra of the samples, as the oxidization time extending, the peak intensity for C6 at 65 ppm decreased gradually, while a new peak at 172 ppm was assigned to C6 carboxyl group. When the oxidation time was more than 80 h, there might be more side reaction on the raw material, and certain degrees of secondary reactions on the hydroxyl groups (C2 and C3). Therefore, the oxidation time should be kept in a reasonable range [25-27]. Consequently, the selectivity oxidation reaction mainly occurs at C6 of a hydroglucose structure [26].

The XRD spectra indicated that both MCC and OMCC belonged to cellulose type I crystalline structure. The

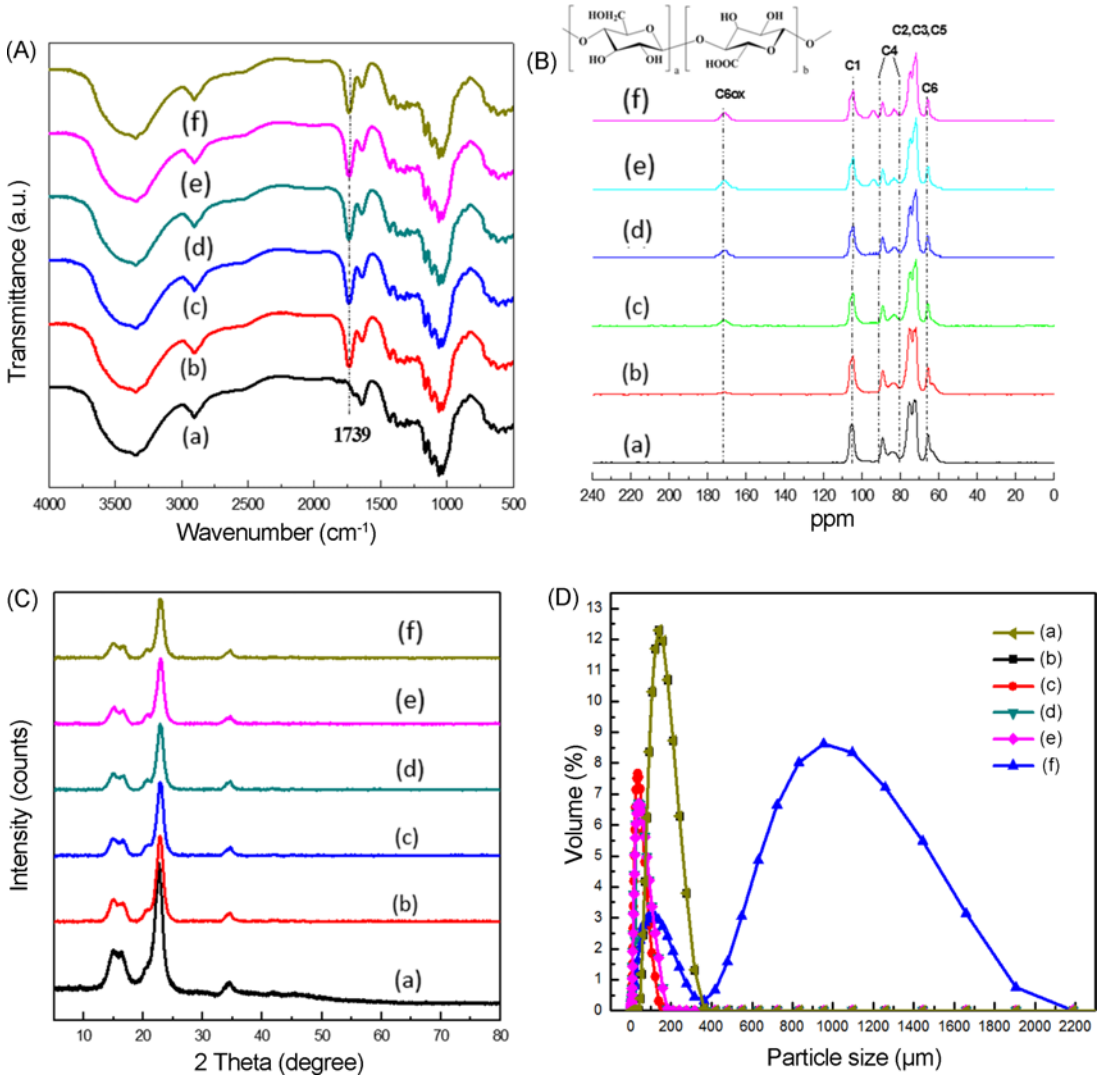

Figure 2. The FTIR spectra (A), ^{13}C solid state NMR Spectra(B), XRD spectra (C) and Particle size (D) for (a) MCC, (b) OMCC-24 h, (c) OMCC-48 h, (d) OMCC-64 h, (e) OMCC-80 h, (f) OMCC-96 h. The selectivity oxidation reaction on MCC mainly occurs at C6 of a glucose structure. The OMCC still belongs to Cellulose type I after oxidation, however the crystallinity and particle size have been decreased.

Table 1. Crystallinity, carboxyl content, DP and Zeta potential values for various samples

Sample	Crystallinity (%)	Carboxyl content (%)	DP	Zeta potential (mV)
MC	70.01±3.56	0	135.00±5.98	-12.91±0.99
ORC	44.36±2.44	18.62±3.22	184.20±4.43	-21.43±2.01
OMCC-24 h	63.24±5.78	8.72±1.93	120.48±5.23	-19.82±0.78
OMCC-48 h	61.83±4.98	10.32±2.01	114.07±4.66	-22.34±1.20
OMCC-64 h	61.66±3.56	16.97±1.98	110.87±3.46	-29.24±1.03
OMCC-80 h	60.93±3.20	18.28±2.21	88.22±5.12	-33.72±1.56
OMCC-96 h	60.36±6.33	19.96±2.14	70.05±3.66	-35.42±1.89
ORC/OMCC-64 h	46.91±4.35	-	-	-23.01±1.24

N=6, X±S, *P<0.05.

crystallinities of OMCC had been calculated from XRD spectra (Table 1). As the oxidation time extended, the values of crystallinity changed from 70.01 % (MCC) to 60.63 % (OMCC-96 h), and the particle size decreased to ca. 80 μm, which may be caused by the oxidization damaged the structure of MCC, meanwhile the oxidization time had little effect on OMCC. The particle sizes of OMCC-96 h had around two different sizes, which was probably caused by the high amount of negative charge resulted in a part of particles conglomerated. The potential and the carboxyl content were both the significant indexes of the OMCC, and as a bio-absorbable hemostatic agent, the carboxyl content must range between 16 % and 24 %. At the same time, the suitable electric charge on the surface of OMCC could rapidly attract and activate the platelets. Table 1 showed that the carboxyl content of OMCC and Zeta potential increased quickly at the beginning. However, the reaction speed of OMCC-64 h, OMCC-80 h and OMCC-90 h reduced gradually when the content reached to a certain value (16.97 %). It was because that when the oxidation reaction in the amorphous region mainly completed, the reaction continued mostly in the surface of crystalline region, subsequently it was difficult to oxidize the hydroxyl groups in the middle of the crystalline region, consequently the carboxyl content reached a balance. The decrease in DP of OMCC was attributed to the time of oxidation. As long as the reaction proceeded (OMCC-80 h and OMCC-96 h), it could be observed that there was a possible secondary reaction on cellulose chains, and the samples were lack of satisfactory mechanical properties and could not be used as biomedical devices. Therefore, OMCC-64 h ought to be the most suitable particle for the hemostatic composite.

The morphology of MCC and OMCC-64 h were both anomalous (Figure 3(A) and Figure 3(B)), while the size of OMCC-64 h was smaller. Figure 3(C) and Figure 3(D) also showed the morphology of the ORC gauze and the ORC/OMCC-64 h hemostatic composite, which indicated that the micro-status of ORC was braided, and there were a bunch of OMCC-64 h particles on the surface of hemostatic composites. This type of structure was helpful to increase the specific surface area, the effective contact area and the storage of blood. From the curve graphs in Figure 3(E), the Brunauer-Emmett-Teller (BET) surface area of ORC, OMCC-64 h, ORC/OMCC-64 h composite were 0.6359 m^2/g, 2.5737 m^2/g, 1.6334 m^2/g, and the adsorption average pore width (4V/A by BET) was 81.2440 Å, 48.2254 Å, 67.9846 Å, respectively. Compared with the ORC gauze, the hemostatic composite had a higher surface area, which could in theory absorb more blood. The ratio of OMCC in composite was 14.74 %, which was calculated from the data of crystallinity.

Biocompatibility and Bioavailability Evaluation

The CCK-8, a colorimetric assay based on tetrazolium dye reduction was used to monitor the relative number of viable cells after 12 h, 24 h and 48 h culture, and the fold change data were showed in Figure 4(A). As the large amount of carboxyl groups on the ORC showed from the NMR results, there was little decrease of cell proliferation at the first 24 h in ORC group. While, for the OMCC-64 h group and ORC/OMCC-64 h, there was a slight increase of cell proliferation at the first 24 h. After cultured for 48 h, the cell proliferations of all groups had an obvious increase, which illustrated that the cells remained viable and had the ability to proliferate normally after treated with ORC, OMCC-64 h or ORC/OMCC-64 h, respectively.

Histopathological examinations of the experimental tissue sites of the subcutaneous implantation showed different responses of the ORC/OMCC-64 h at different implanted periods. In sites where the ORC/OMCC-64 h was applied for 2 weeks, the material could be found still on some of the sections, which were unstained by HE. In Figure 4(B), there were obvious capsules composed of many lymphocytes, eosinophils and tissue cells around the samples and the thicknesses of these capsules were dozens to hundreds of micrometers. As the implanted period lasted for 4 weeks, neither the residual testing ORC/OMCC-64 h composite nor

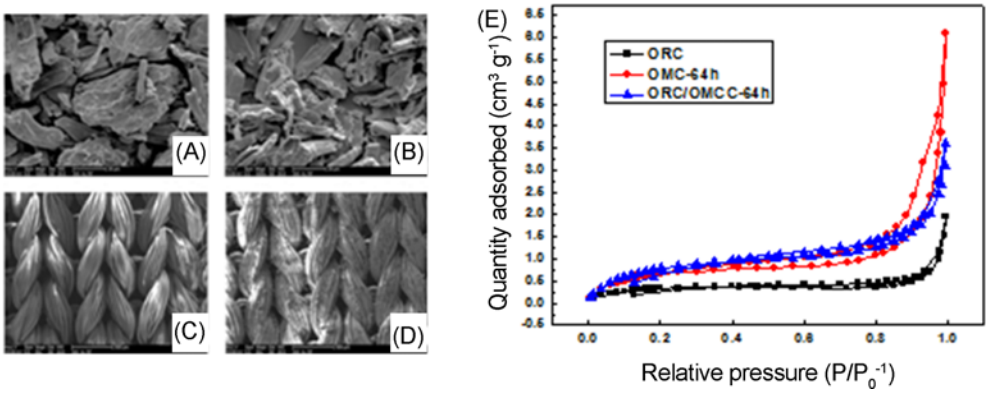

Figure 3. The SEM images of (A) MC, (B) OMCC-64 h, (C) ORC gauze, (D) hemostatic composite (ORC/OMCC-64 h). The nitrogen adsorption-desorption isotherm of ORC, OMCC-64 h, ORC/OMCC-64 h composite (E).

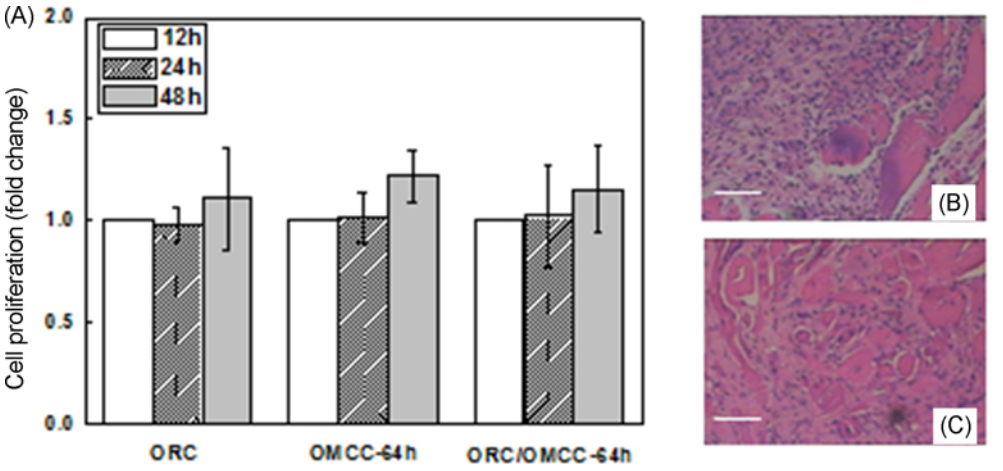

Figure 4. Cell proliferation (A) on TCPs cultured for 12 h, 24 h and 48 h in DMEM with different material extracting solutions (material/PBS, 1 g/1 m*l*, w/v). Photomicrographs of ORC-OMCC-64 h composite on subcutaneous implantation site for 2 week (B) and 4 week (C). The scar bar is 100 μm.

Table 2. The median values for hemostatic time and blood loss of different materials in the two trauma models

	Middle ear artery model		Hepatic trauma model	
	Hemostatic time (s)	Blood loss (g)	Hemostatic time (s)	Blood loss (g)
Gauze	>600	-	>600	-
ORC	178±48*	2.197±0.325*	257±33*	4.102±0.825*
OMCC-64 h	151±32*	1.564±0.253*	176±42*	3.629±0.724*
ORC/OMCC-64 h	131±42*	1.456±0.523*	173±22*	2.899±0.732*

N=6, X±S, *P<0.05.

the obvious anaphylactic tissue reactions were observed in the implantation sites (Figure 4(C)), which demonstrated that the ORC/OMCC-64 h could be degradated in vivo after implatated for 4 weeks. Combined with the CCK results and biodegradation text, it was proved that the ORC-OMCC-64 h had a good biocompatibility with both the cells and the animals.

After placing different samples on the middle ear artery or the hepatic trauma on liver lobes of rabbits, the samples were soaked with blood and turn to dark brown or black immediately, and then gradually formed a clot. The blood loss was affected by a number of factors such as weight, age, blood pressure of the rabbits. From Table 2, it was seen that the gauze had low hemostatic property, as it had no ability to stop bleeding within 600 s. It was noteworthy that the ORC covering on the liver would help the subtraction of the average hemostatic time and the blood loss. In rabbit ear artery injury model, the hemostatic speed of ORC/OMCC-64 h composite (131±42 s) was faster than the ORC (178±48 s) and OMCC-64 h (151±32 s). The difference was statistically significant as P<0.05. It was showed that the amount of bleeding of ORC/OMCC-64 h composite (1.456±0.523 g) was less than the ORC group with a value of 2.197±0.325 g, OMCC-64 h group with a value of 1.564±0.253 g (P<0.05). In rabbit liver injury model, the hemostatic time of three materials (ORC, 257±33 s; OMCC-64 h, 176±42 s and ORC/OMCC-64 h composite, 173±22 s) were significantly less than the Gauze group (>600 s). The difference was statistically significant as P<0.05. The amount of bleeding of ORC was 4.102±0.825 g, and the value of OMCC-64 h was 3.629± 0.724 g. The lowest one was ORC/OMCC-64 h composite (2.899±0.732 g), which was significant different with ORC and OMCC-64 h (P<0.05). In brief, the composite exhibited prominent hemostatic property in the aspect of shorter average hemostatic time and the less blood loss.

The antibacterial performances of these samples had been evaluated by using Gram-positive bacterium (*S. aureus*) and Gram-negative bacterium (*E. coli*). Reduction of CFU was calculated in order to estimate the antibacterial efficiency. The reduction of CFU for ORC, OMCC-64 h and the hemostatic composite (ORC/OMCC-64 h) all exceeded 99.9 %. It indicated that comparing to the control group and normal gauze, all of the samples with carboxyl group had good antibacterial activity.

Blood Analysis in vitro

Blood coagulation process was composed of intrinsic coagulation and extrinsic coagulation, and the difference

Table 3. The reduction in CFU of different materials

Sample	Control	Normal gauze	ORC	OMCC-64	ORC/ OMCC-64
CFU (%)	12.4	19.3	>99.9	>99.9	>99.9

between them was their different pathway of activating coagulation factors. The intrinsic coagulation pathway means the coagulation factors all come from the blood [28]. This activation is usually caused by the surface contact between blood and foreign matters with negative charge, then the intrinsic coagulation system starts with the factor XII activation. On the other hand, the extrinsic coagulation pathway refers to the part of coagulation factors coming from the organization, and it begins from the activation of factor III, VII [29].

The data of blood coagulation text and platelets adhesion assay from Table 3 indicated that, for hemostatic composite, there was the maximal influence on APTT & TT value and the highest platelets adhesion rate. With the increasing of concentration, the values of APTT & TT were decreasing fast. However, the platelets adhesion rate was rapidly increasing, and there was no obvious effect on PT value. The samples would have hemostatic effects only if the concentrations of them had reached a certain level, which was to say, they had concentration dependence.

The tiny changes for the concentrations of different blood coagulation factors were determined by ELISA. The concentrations of β-TG (Figure 5(B)) and PF4 (Figure 5(A)) released after platelets activation were 776.39 pg/m*l* (S.D. 20.12 pg/m*l*) and 6.19 ng/m*l* (S.D. 0.34 ng/m*l*) in the control group (withour any samples in blood). After adding gauze, the factors both had the marked release ($P<0.05$), reached to 1492.77 pg/m*l* (S.D.31.23 pg/m*l*, β-TG) and 9.61 ng/m*l* (S.D. 0.26 ng/m*l*, PF4), respectively. Furthermore, after adding ORC powders, the factors both increased slightly ($P<0.05$), reached to 1598.49 pg/m*l* (S.D. 33.81 pg/m*l*, β-TG) and 9.97 ng/m*l* (S.D. 0.40 ng/m*l*, PF4), respectively. The factor concentrations of OMCC-64 h (1766.82 pg/m*l*, S.D. 23.45 pg/m*l*, β-TG; and 10.22 ng/m*l*, S.D. 0.21 ng/m*l*, PF4) had a smaller decline than these of hemostatic composite (1803.68 pg/m*l*, S.D.39.02 pg/m*l*, β-TG; and 10.46 ng/m*l*, S.D. 0.39 ng/m*l*, PF4). The average determination results of GP IIb/IIIa (Figure 5(B)) which could reveal the activation of platelets glycoprotein were respectively 11.65 ng/m*l* (S.D. 0.46 ng/m*l*, control group), 16.02 ng/m*l* (S.D. 0.48 ng/m*l*, add gauze) and 17.46 ng/m*l* (S.D. 0.31 ng/m*l*, add ORC-40 h), 19.35 ng/m*l* (S.D. 0.33 ng/m*l*, 19.65 ng/m*l* (S.D. 0.42 ng/m*l*, and it proved that the OMCC and hemostatic composite had an equal strong activation on platelets. The FXIIa had been measured (Figure 5(A)), which was able to make clear the progress of hemostasis starting with the intrinsic coagulation. The concentration of FXIIa in human blood was obviously raised, and the average value of control group, gauze, ORC, OMCC-64 h and hemostatic composite were 41.23 U/*l* (S.D. 2.15 U/*l*), 67.35 U/*l* (S.D. 3.21 U/*l*), 72.15 U/*l* (S.D. 3.32 U/*l*), 78.24 U/*l* (S.D. 3.55 U/*l*), and 82.51 U/*l* (S.D. 4.23 U/*l*), respectively. And the results of GP IIb/IIIa and FXIIa for the samples all had the significant differences from the control group ($P<0.05$).

Possible Mechanism of the Hemostasis for Hemostatic Composite

The hemostatic mechanism of hemostatic composite

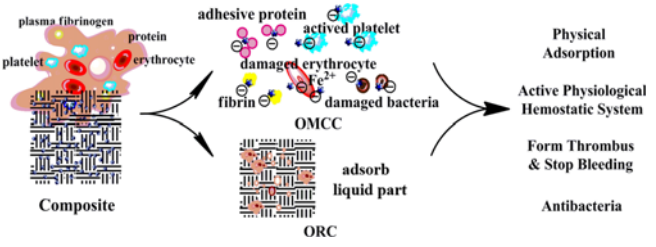

Scheme 1. Schematic diagram of the hemostasis mechanism.

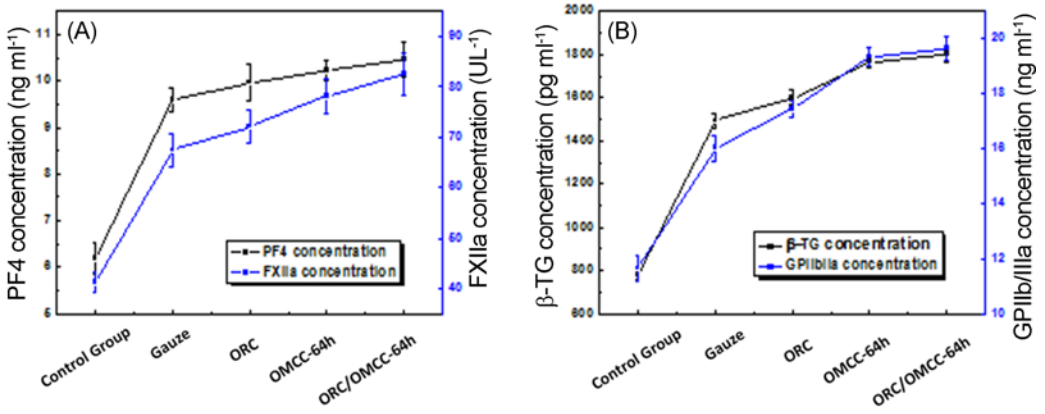

Figure 5. The Effecting trend of different samples to the various factors. The release of PF4 (A) and β-TG (B) are enhanced only after platelets activated. Factor FXIIa (A) increase plays an important role to start the intrinsic coagulation pathway. The concentration of GP IIb/IIIa (B) increases when the activated platelets aggregate.

Table 4. The values of APTT, TT, PT and platelets adhesion rate for different samples in vitro

Sample	APTT (s)			TT (s)			PT (s)			Platelets adhesion rate (%)		
Concentration	2 %	1 %	0.5 %	2 %	1 %	0.5 %	2 %	1 %	0.5 %	2 %	1 %	0.5 %
Control group		38.3±4.1			18.1±3.3			11.5±0.8			-	
Gauze	35.3±3.4	37.2±2.1	38.6±2.9	15.3±0.7	16.6±0.6	17.3±1.6	12.3±0.1	11.7±0.9	12.1±0.2	15.1±7.6	10.3±1.6	9.7±2.4
ORC	29.9±2.7	33.8±0.4	36.3±2.5	14.7±0.5	15.9±1.9	16.3±0.9	11.8±0.4	11.5±0.8	12.2±0.2	30.1±8.4	27.3±6.2	19.9±8.5
OMCC-64 h	26.3±1.8	29.5±1.3	32.5±1.7	13.3±0.3	13.8±1.6	15.8±0.7	12.2±0.2	12.1±0.2	11.7±0.5	35.5±1.8	33.7±9.1	21.2±7.3
ORC/OMCC-64 h	25.8±3.2	27.1±3.9	31.9±4.2	12.6±1.0	13.9±0.7	15.1±0.4	12.1±0.4	11.8±0.3	12.0±0.4	46.4±5.1	42.1±8.8	30.4±3.7

N=6, X±S, *P<0.05.

(shown in Scheme 1) is a combination of physical adsorption and the physiological hemostasis. When the hemostatic composite with larger specific surface area is applied to the bleeding wound, the ORC base part could absorb most of the liquid in the blood. The OMCC particles with electric charge on its surface are exposed, which could rapidly adhere protein and damaged erythrocytes. The iron atom at the ferrous state from the damaged erythrocytes have strong complexation ability to the carboxyl groups on OMCC, which leads to nonspecific aggregation of blood cells or small molecules and generating a blood clot [30]. This amplification mechanism will be important for the formation of stable platelets thrombi at sites of vascular injuries, especially in the venous vessels.

From ELISA analysis of the OMCC, the concentrations of β-TG and PF4 increase after platelets are activated, and the platelet glycoprotein (GPIIb/IIIa) receptor becomes competent to stimulate the release of cellular grain and secretion, including all sorts of clotting factors [31]. The data of Table 4 can indicate this opinion. ORC, OMCC and hemostatic composite all have the effects on the activation of factor VIII, IX, XI, XII, and have no effect on the activation of factor III, VII, so just the intrinsic coagulation system is activated. Expecially, this can greatly accelerate the activation of the blood coagulation factor XII, and promote the generation of thrombin [32,33]. In the presence of thrombin, the soluble fibrinogen changes to solid fibrin quickly, which can arouse hemostatic action effectively. Meanwhile, this could make the platelets adhesion rate high to form the thrombus on the damaged blood vessels to fill the damaged organization and stop bleeding [34].

As we all know, the negative charge is able to damage the cell membrane of bacteria. On the other hand, the carboxyl of ORC or OMCC can be subject to multiple chemical reactions, such as generating amide structure or ester group structure, which can disturb the normal metabolism of bacteria. Thus, this hemostatic composite also have good bacteriostasis.

Conclusion

In this article, we prepared the OMCC particles by a simple and effective method from MCC which is one of the most important products from lignocellulose using less oxidation liquid than ORC. In the meantime, the OMCC had the great physio-chemical properties and biological properties as a hemostatic material. The data analysis of the FTIR and NMR showed that the NO_2/CCl_4 oxidation system had a high selectivity on hydroxyl group at C6 of MCC, and the OMCC particles exhibited negative charges which were attributed to the carboxyl groups. Among various chemical and physical tests, the OMCC-64 h was the most suitable particle to combine with ORC to prepare a novel hemostatic composite, which had the good properties for hemostasis and bacteriostasis from the bioavailability evaluation. The possible mechanism of the ORC/OMCC-64 h composite was explored using blood coagulation text, platelets adhesion assay and ELISA. It was demonstrated that this process was a combination of physical adsorption and the physiological hemostasis, which were aroused from the super BET surface area and the stimulation for the intrinsic coagulation factors. In the future, our lab will focus on how to prepare much smaller hemostatic materials with nanostructures and composite different hemostatic materials with complementary properties by simple methods.

Acknowledgement

This work was financially supported by Weihai Science and Technology Development Plan Project (2013GNS028), China Postdoctoral Science Foundation Project (2013M541372).

References

1. A. Pinkert, K. N. Marsh, S. Pang, and M. P. Staiger, *Chem. Rev.*, **109**, 6712 (2009).
2. A. Isogai, T. Saito, and H. Fukuzumi, *Nanoscale*, **3**, 71 (2011).
3. D. O. Carlsson, J. Lindh, L. Nyholm, M. Strømme, and A. Mihranyan, *RSC Adv.*, **4**, 52289 (2014).
4. Q. Cui, Y. Zheng, Q. Lin, W. Song, K. Qiao, and S. Liu, *RSC Adv.*, **4**, 1630 (2014).
5. T. Saito, S. Kimura, Y. Nishiyama, and A. Isogai, *Biomacromolecules*, **8**, 2485 (2007).

6. X. Shi, Q. Fang, M. Ding, J. Wu, F. Ye, Z. Lv, and J. Jin, *J. Biomater. Appl*., **30**, 1092 (2016).
7. C. Moser and W. Ashton, *U .S. Patent*, 3364200 (1968).
8. G. Banker and V. Kumar, *U. S. Patent*, 5414079 (1995).
9. W. Cheng, J. He, Y. Wu, C. Song, S. Xie, Y. Huang, and B. Fu, *Cellulose*, **20**, 2547 (2013).
10. Y. Wu, J. He, W. Cheng, H. Gu, Z. Guo, S. Gao, and Y. Huang, *Carbohydr. Polym*., **88**, 1023 (2012).
11. H. Gu, J. He, Y. Huang, and Z. Guo, *Fiber. Polym*., **14**, 1266 (2013).
12. W. K. Son, J. H. Youk, and W. H. Park, *Biomacromolecules*, **5**, 197 (2004).
13. M. K. M. Haafiz, A. Hassan, Z. Zakaria, and I. M. Inuwa, *Carbohydr. Polym*., **103**, 119 (2014).
14. S. Kamel, N. Ali, K. Jahangir, S. M. Shah, and A. A. El-Gendy, *Exp. Polym. Lett*., **2**, 758 (2008).
15. R. Pönni, T. Vuorinen, and E. Kontturi, *BioResources*, **7**, 6077 (2012).
16. P. E. Knight, F. Podczeck, and J. M. Newton, *J. Pharm. Sci.*, **98**, 2160 (2009).
17. A. A. Baker, W. Helbert, J. Sugiyama, and M. J. Miles, *Appl. Phys. A Mater. Sci. Process*., **66**, S559 (1998).
18. S. J. Eichhorn and R. J. Young, *Cellulose*, **8**, 197 (2001).
19. Q. Wu, M. Henriksson, X. Liu, and L. A. Berglund, *Biomacromolecules*, **8**, 3687 (2007).
20. J. V. Edwards, N. J. Castro, B. Condon, C. Costable, and S. C. Goheen, *J. Biomater. Appl*., **26**, 939 (2012).
21. M. A. S. A. Samir, F. Alloin, and A. Dufresne, *Biomacromolecules*, **6**, 612 (2005).
22. H. Liu, D. Wang, Z. Song, and S. Shang, *Cellulose*, **18**, 67 (2011).
23. S. S. Wong, S. Kasapis, and Y. M. Tan, *Carbohydr. Polym*., **77**, 280 (2009).
24. C. C. Conrad and A. G. Scroggie, *Ind. Eng. Chem.*, **37**, 592 (1945).
25. S. Fujisawa, Y. Okita, H. Fukuzumi, T. Saito, and A. Isogai, *Carbohydr. Polym*., **84**, 579 (2011).
26. A. Isogai, T. Saito, and H. Fukuzumi, *Nanoscale*, **3**, 71 (2011).
27. I. Siró and D. Plackett, *Cellulose*, **17**, 459 (2010).
28. D. Gailani and T. Renné, *Arterioscler. Thromb. Vasc. Biol*., **27**, 2507 (2007).
29. N. Mackman, R. E. Tilley, and N. S. Key, *Arterioscler. Thromb. Vasc. Biol*., **27**, 1687 (2007).
30. B. Martina, K. Kateřina, R. Miloslava, G. Jan, and M. Ruta, *Adv. Polym. Technol*., **28**, 199 (2009).
31. S. Coseri, G. Biliuta, B. Simionescu, K. S. Kleinschek, V. Ribitsch, and V. Harabagiu, *Carbohydr. Polym*., **93**, 207 (2013).
32. C. Schonauer, E. Tessitore, G. Barbagallo, V. Albanese, and A. Moraci, *Eur. Spine. J.*, **13**, S89 (2004).
33. S. Keshavarzi, M. MacDougall, D. Lulic, A. Kasasbeh, and M. Levy, *Wounds*, **25**, 160 (2013).
34. A. C. Brown and T. H. Barker, *Acta Biomaterialia*, **10**, 1502 (2014).